HHS Public Access

Author manuscript

*ACS Appl Mater Interfaces*. Author manuscript; available in PMC 2019 April 11.

Published in final edited form as:

*ACS Appl Mater Interfaces*. 2018 April 11; 10(14): 11495–11507. doi:10.1021/acsami.7b19708.

# Effects of Nanoprobe Morphology on Cellular Binding and Inflammatory Responses: Hyaluronan-Conjugated Magnetic Nanoworms for Magnetic Resonance Imaging of Atherosclerotic Plaques

**Seyedmehdi Hossaini Nasr**[†], **Anne Tonson**[‡], **Mohammad H. El-Dakdouki**[†,§], **David C. Zhu**[‖], **Dalen Agnew**[⊥], **Robert Wiseman**[‡,‖], **Chunqi Qian**[*,‖], and **Xuefei Huang**[*,†,#,⊗]

[†]Department of Chemistry, Michigan State University, East Lansing, Michigan 48824, United States

[‡]Department of Physiology, Michigan State University, East Lansing, Michigan 48824, United States

[‖]Department of Radiology, Michigan State University, East Lansing, Michigan 48824, United States

[⊥]Department of Pathobiology and Diagnostic Investigation, Michigan State University, East Lansing, Michigan 48824, United States

[#]Department of Biomedical Engineering, Michigan State University, East Lansing, Michigan 48824, United States

[⊗]Institute for Quantitative Health Science and Engineering, Michigan State University, East Lansing, Michigan 48824, United States

[§]Department of Chemistry, Beirut Arab University, P.O. Box 11-5020, Riad El Solh 11072809, Beirut, Lebanon

## Abstract

Atherosclerosis is an inflammatory disease of arterial walls and the rupturing of atherosclerotic plaques is a major cause of heart attack and stroke. Imaging techniques that can enable the detection of atherosclerotic plaques before clinical manifestation are urgently needed. Magnetic resonance imaging (MRI) is a powerful technique to image the morphology of atherosclerotic plaques. In order to better analyze molecular processes in plaques, contrast agents that can selectively bind to plaque receptors will prove invaluable. CD44 is a cell surface protein

[*]Corresponding Authors: xuefei@chemistry.msu.edu. qianchu1@msu.edu.

**ORCID**

Chunqi Qian: 0000-0003-4528-4572

Xuefei Huang: 0000-0002-6468-5526

**Notes**

The authors declare no competing financial interest.

Supporting Information

The Supporting Information is available free of charge on the ACS Publications website at DOI: 10.1021/acsami.7b19708. Relaxivity measurements, HA removal by gel electrophoresis, thermogravimetric analysis, CD44 Western blotting, flow cytometry data, HA-NW cellular uptake for different doses, blood chemistry panel data, MRI data (PDF)

overexpressed in plaque tissues, the level of which can be correlated with the risks of plaque rupture. Thus, targeting CD44 is an attractive strategy for detection of atherosclerotic plaques. Herein, we report the synthesis of hyaluronan-conjugated iron oxide nanoworms (HA-NWs). A new purification and gel electrophoresis protocol was developed to ensure the complete removal of free HA from HA-NWs. Compared to the more traditional spherical HA-bearing nanoparticles, HA-NWs had an elongated shape, which interacted much stronger with CD44-expressing cells in CD44- and HA-dependent manners. Furthermore, the HA-NWs did not induce much inflammatory response compared to the spherical HA nanoparticles. When assessed in vivo, HA-NWs enabled successful imaging of atherosclerotic plaques in a clinically relevant model of ApoE knockout transgenic mice for noninvasive plaque detection by MRI. Thus, nanoprobe shape engineering can be a useful strategy to significantly enhance their desired biological properties.

## Graphical Abstract

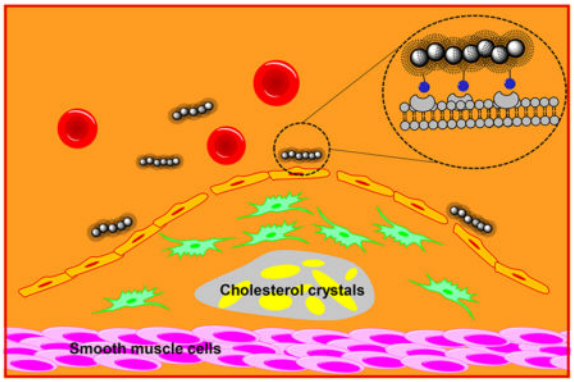


### Keywords

ApoE knockout mice; atherosclerosis; hyaluronan; magnetic resonance imaging; nanoworms

## INTRODUCTION

Atherosclerosis, the thickening of arterial vessel walls as a result of invasion and accumulation of inflammatory cells and lipids, is a major cause of heart attacks and strokes.[1] The majority of patients that experience cardiac arrests have atherosclerosis. Early detection via noninvasive methods is highly attractive to guide the prevention and the treatment of this disease.[2,3]

Imaging of atherosclerotic plaques is an active area of research.[4,5] Compared to techniques such as positron emission tomography (PET) and/or computed tomography (CT), magnetic resonance imaging (MRI) is advantageous as it does not use ionizing radiation while giving superior spatial resolution in vivo.[6,7] Furthermore, contrast agents can be developed to enhance the sensitivity of atherosclerotic plaque detection by MRI.[8,9] There are two general classes of contrast agents. The first are passive agents, which can diffuse into plaques or be taken up by macrophages capable of trafficking to plaques. The second are active agents

designed to bind with receptors overexpressed by plaques, enabling selective accumulation in plaques and contrast changes from surrounding tissues.

To achieve active targeting, the selection of a suitable receptor target is important. CD44 is a cell surface receptor critical for recruitment of inflammatory cells to atherosclerotic plaques.[10,11] In histological analysis of atherosclerotic plaques in both humans and an atherosclerotic animal model, i.e., ApoE knockout mice, CD44 has been found to be expressed at much higher levels (>10 fold) in plaque regions that are prone to rupture compared to those in healthy vascular tissues.[10,12–14] Knocking down CD44 expression levels in ApoE knockout mice reduced aortic lesions for more than 50%.[12]

The major endogenous ligand for CD44 is the polysaccharide hyaluronan (HA).[15,16] CD44 is normally kept in a quiescent state with low HA affinity. However, in the presence of inflammatory signals such as TNF-$\alpha$ that are common in atherosclerotic plaques, post-translational modification of CD44 occurs, switching it to a high-affinity state for strong HA binding.[11,17] Thus, HA can be a useful ligand to target CD44 and sense inflammation in atherosclerotic plaques.[18–21] We synthesized HA-coated super paramagnetic iron oxide nanoparticles (HA-SPIONs), which have been used to image atherosclerotic plaques in rabbits by MRI.[19] One potential concern of a SPION-based system is the inflammatory activity. Herein, we report that engineering the spherical shape of HA-SPIONs to wormlike structures of HA-nanoworms (HA-NWs) can significantly reduce their inflammatory activities. Furthermore, HA-NWs have much higher binding avidity with CD44-expressing cells. This new nanoprobe enables successful noninvasive detection of atherosclerotic plaques by MRI in ApoE knockout mice, a suitable model of human atherosclerosis diseases. This work highlights the significant impacts morphology can have on biological functions of nanoprobes.

## MATERIALS

Iron(III) chloride hexahydrate ($FeCl_3 \cdot 6H_2O$) was purchased from Honeywell Riedel-de Haën. Iron(II) chloride tetrahydrate ($FeCl_2 \cdot 4H_2O$), dimethyl sulfoxide (DMSO), dextran (MW: 10 and 40 kDa), formalin solution neutral buffered 10%, fetal bovine serum (FBS), Dulbecco's phosphate-buffered saline (DPBS), Dulbecco's Modified Eagle Medium (DMEM), anti-CD44 antibody [MEM-85] and Amberlite IR 120 hydrogen form (Amberlite $H^+$) were ordered from Sigma-Aldrich. Ultrafiltration disk (100 kDa) and centrifugal filter MWCO (100 kDa) were purchased from EMD Millipore. 2-Chloro-4,6-dimethoxy-1,3,5-triazine (CDMT) and *N*-methylmorpholine (NMM) were purchased form Acros Organics. Sodium hyaluronan (30 kDa) was obtained from Lifecore Biomedicals. Ammonium sulfate was purchased from Chempure Chemicals. Fluorescein isothiocyanate (FITC), 4′,6-diamidino-2-phenylindole (DAPI), LysoTracker-594 DND, and TURBO DNA-free Kit were purchased from Invitrogen. Penicillin–streptomycin (Pen Strep) mixture, trypsin–EDTA (0.5%), Power SYBR Green PCR Master Mix, and L-glutamine were obtained from Thermo-Fisher. EA.hy926 and SKOV-3 cells were ordered from the American Tissue Culture Collection (ATCC). Goat antimouse HRP antibody was purchased from Biorad. HyGLO chemiluminescent HRP antibody detection reagent was purchased from Denville Scientific. Nitric acid TraceMetal grade and ammonium hydroxide were obtained from

Fisher Scientific. Recombinant human (rh) CD44 was ordered from R&D Systems. Mouse IgG2b antibody (PLPV219) was purchased from Abcam. RNeasy Mini Kit was ordered from QIAGEN. dNTP Mix, GoScript Reverse Transcriptase, Random Primers and CellTiter 96 Aqueous One solution containing 3-(4,5-dimethylthiazol-2-yl)-5-(3-carboxymethoxyphenyl)-2-(4-sulfophenyl)-2*H*-tetrazolium (MTS) were purchased from Promega. TNF alpha mouse ELISA kit and IL-1 beta mouse ELISA kit were ordered from Thermo-Fisher.

## Synthesis of HA-NWs

Nanoworms (NWs) were prepared using $Fe^{2+}$ and $Fe^{3+}$ salts in the presence of dextran.[22] Briefly, dextran (2.35 g, MW40 kDa), $FeCl_3 \cdot 6H_2O$ (1.17 mmol) and $FeCl_2.4H_2O$ (0.63 mmol) were dissolved in MQ water (4.5 mL) under purge of Ar. Concentrated aqueous ammonia (0.5 mL) was then added dropwise to the reaction flask under vigorous stirring and a steady purge of Ar. It was then heated slowly up to 70 °C over 1 h and held at this temperature for an additional hour. After being cooled to room temperature, the reaction mixture was diluted to 300 mL and washed using an ultrafiltration system (MWCO 100000) 5 times to remove ammonium chloride salts and the excess amount of the base. The resulting NWs were concentrated to 30 mL and then cross-linked by adding sodium hydroxide solution (5 M, 10 mL) and epichlorohydrin (ECH) (5 mL) under Ar flow and fast stirring for 24 h. The reaction mixture was dialyzed against water followed by ultrafiltration 5 times to remove the excess amount of ECH. To functionalize cross-linked NWs by amine groups for further conjugation, cross-linked NWs were first concentrated to 30 mL, and then concentrated 30% ammonium hydroxide in water (10 mL) was added. The mixture was stirred vigorously for 36 h at 37 °C. Finally, amine-functionalized NWs were washed by dialysis against distilled water three times (12 h each) to remove the excess base.

HA conjugation with NWs were performed through NMM and CDMT chemistry.[18] First, sodium hyaluronan (MW 31 kDa, 100 mg) was dissolved in MQ water (5 mL) then the pH was brought to 3 by adding Amberlite $H^+$ resin and it was stirred for 4 h. The resin was removed by filtration and the mixture was freeze-dried. The protonated HA (74 mg, 0.19 mmol carboxylic acid) was dissolved in MQ water (3 mL) followed by dropwise addition of acetonitrile (2 mL). Then, NMM (22 $\mu$L, 0.2 mmol) and CDMT (18 mg, 0.10 mmol) were added to this HA solution. The reaction mixture was stirred at room temperature for 1 h followed by addition of an aqueous dispersion of NWs (30 mg) and further stirring for 36 h under nitrogen. HA-NWs were washed by ultrafiltration (MW 100,000) 5 times and stored for future experiments. HA-NWs were labeled with fluorescein isothiocyanate (FITC) by dissolving FITC (5 mg) in DMSO (2 mL) and adding this mixture to an aqueous solution of HA-NWs (70 mg in 10 mL water). The reaction mixture was stirred in dark for 48 h then unreacted FITC was washed off through dialysis (5 times) in water and PBS buffer.

## Characterization and Physicochemical Properties of HA-NWs

Following each step of NP synthesis, the size and charge of the NPs were measured by dynamic light scattering (DLS) using a Zetasizer Nano zs apparatus (Malvern, U.K.). The prepared NPs were imaged under transmission electron microscope (TEM) (JEM-2200FM) operating at 200 kV using Gatan multiscan CCD camera with Digital Micrograph imaging

software. Thermal gravimetric analysis (TGA) was performed to quantify the total amount of organic content of NPs. Magnetic relaxivities ($r_2$* and $r_1$) were measured in a 7 T magnet.

### Purification of HA-NWs

HA-NWs were washed with a concentrated ammonium sulfate solution (35%) through centrifugal filters (MWCO: 100 kDa). They were then transferred to a dialysis bag (MWCO: 3 kDa) to remove the excess salt through multiple exchanges (6 times) of distilled water. After purification, a modified electrophoresis gel staining method was used to enable visualization of HA in each sample.[23] Briefly, an agarose gel (0.8%) was prepared and samples containing HA-NWs both before and after purification containing the same amounts of Fe (40 μg) and free HA (70 μg) were loaded on the gel. Before loading, each sample was mixed with 5 μL of sucrose solution (2 M) and 2 μL of bromophenol blue solution. The gel electrophoresis was run at 150 V for 70 min. Next, the gel was placed in a freshly prepared Stains-All dye solution (0.005%) in 50% ethanol for 24 h in dark. Gels were destained in the dark using 10% ethanol solution and the ethanol mixture was exchanged every 12 h until the purple color washed off from the gel.

### Verifying CD44 Expression on Cells

Cells were grown in a 100 mm × 20 mm Petri dish until 80% confluence was reached. The cell culture medium was removed, and cells were washed twice with PBS. Then lysis buffer, prepared by mixing 500 μL of RIPA buffer, protease inhibitor cocktail and 2.5 μL of phenyl methyl sulfonyl chloride (PMSF), was added to the cells while the Petri dish was kept on ice for about 15 min until cell debris started to float around. Then cell lysates were collected by a cell scraper, transferred to an Eppendorf tube, and homogenized using a probe homogenizer. Protein content was quantified by a Bradford assay. Different concentrations of the lysates were loaded on a nonreducing gel (stacking gel:18%; resolving gel: 10%) with rhCD44 protein as the standard. The gel was subjected to electrophoresis (200 V) for 60 min, and the blots were then transferred to PVDF membrane (60 V) for 90 min. After the membrane was blocked using 4% nonfat milk in TBS-tween (TBST) buffer, the membrane was first treated with mouse anti human CD44 mAb (MEM 85) diluted to 1:1000 in 4% nonfat milk in TBST at 4 °C overnight followed by goat antimouse HRP antibody (secondary Ab) for 1 h. The membrane was sprayed with a chemiluminescent HRP detection reagent and developed onto autoradiography film.

### HA-NW Uptake by CD44 Expressing Cells

Human vascular endothelial cells (EA.hy926) were used to evaluate the uptake of FITC-HA-NWs. Cells were suspended in a six-well plate over a cover glass at a density of $10^5$ cells per mL and incubated overnight at 37 °C with 5% $CO_2$ to adhere on cover glass and wells. After the medium was removed and the cells were washed with PBS buffer, a solution of FITC-HA-NWs (200 μg/mL) or FITC-HA-SPIONs (220 μg/mL) in DMEM without FBS was added to the cells. Both samples were adjusted to have the same fluorescence intensities. After 1 h of incubation, Lysotracker Red (1 μM, 50 μL/well) was added, and the plate was incubated for another 1 h. The supernatant was removed, and the cells were washed three times with PBS buffer. The cells were fixed by adding 10% formalin (1 mL/well), and after 15 min, formalin was removed and cells were washed with PBS buffer (three times). DAPI

solution (300 nM, 300 μL/well) plus 200 μL of PBS buffer were added to each well. After 4 min, they were removed, and cells were washed five times with PBS buffer. The cover glass was placed on a microscope slide, and images were obtained by Olympus FluoView 1000 LSM confocal microscope.

### Dose-Dependent Cellular Uptake of HA-NWs

To evaluate dose-dependent uptake of HA-NWs by SKOV-3 cells, media with different concentrations of HA-NWs were prepared (5, 10, 20, 50, 100, 200, and 400 μg Fe/ml) and incubated with cells for 1 h. Then, the medium was removed, and cells were washed with PBS buffer five times to remove any unbound particles. Finally, cells were collected and treated with concentrated nitric acid for 2 h at 60 °C followed by addition of a diluted nitric acid (2%) solution. Fe content of each sample was analyzed by Inductively Coupled Plasma–Atomic Emission Spectroscopy (ICP–AES).

### Time-Dependent Cellular Uptake of HA-NWs

EA.hy926 cells were cultured in a six-well plate at 37 °C and 5% $CO_2$ until they became confluent. Then FITC-HA-NWs (50 μg/mL) were added to the cells and allowed to incubate for 1, 2, and 4 h. Next, the medium was removed, and the cells were washed with PBS three times. Then trypsin was used to detach the cells, and it was neutralized by adding 5 volumes of serum-containing DMEM. Finally, cells were collected by centrifugation (1600 rpm, 5 min), resuspended in DMEM, and transferred to FACS tube and kept on ice until FACS analysis.

### HA-NW Binding with CD44 Expressing Cells by FACS Analysis

To assess the binding of FITC-HA-NWs with CD44-expressing cells, human ovarian cancer cells (SKOV-3) were cultured in a six-well plate ($3 \times 10^5$ cells/well) and incubated at 37 °C and 5% $CO_2$ until the cells became confluent. Cells were washed with PBS then FITC-HA-NWs (100 μg/mL), and FITC-HA-SPIONs (110 μg/mL) at equivalent fluorescence amounts were dispersed in serum-free DMEM and added to the cells and incubated for 1 h at 37 °C and 5% $CO_2$. Medium was removed and cells were washed with PBS three times. Cells were detached by adding trypsin, neutralized by adding five volumes of serum-containing DMEM, centrifuged (1600 rpm, 5 min), resuspended in DMEM, and transferred to FACS tubes kept on ice until FACS analysis.

### HA-NW Binding with CD44 Expressing Cells by ICP Analysis

To evaluate the binding of HA-NWs with CD44-expressing cells by ICP-AES, the amount of Fe was measured after treatment of cells with HA-NWs and HA-SPIONs for 1 h. Cells were cultured in a six-well plate($3 \times 10^5$ cells/well) and incubated at 37 °C and 5% $CO_2$ until the cells became confluent. Then the medium was removed, and cells were washed with PBS buffer. HA-NWs (50 μg Fe/mL) and HA-SPIONs (50 μg Fe/mL) were dispersed in DMEM without FBS, added to the cells, and incubated for 1 h. Next, medium was removed, and cells were washed with PBS buffer three times. Cells were collected, 2 mL of concentrated $HNO_3$ was added, and it was stored at 60 °C for 2 h. Finally, each sample was diluted with $HNO_3$ solution (2%), and its Fe content was measured using ICP-AES.

### Verifying the Role of HA in HA-NW Binding with CD44-Expressing Cells

To study the role of HA in binding of HA-NWs with CD44-expressing cells, FITC-labeled NWs (FITC-NWs) were prepared and SKOV-3 cells were treated with equivalent fluorescence amounts of FITC-HA-NWs and FITC-NWs for 45 min. Then the medium was removed, and cells were washed with PBS buffer three times. Next, cells were detached by adding trypsin and then neutralized by addition of 5 volumes of serum-containing DMEM. Finally, cells were collected by centrifugation (1600 rpm, 5 min), resuspended in DMEM, transferred to a FACS tube, and kept on ice until FACS analysis.

### Establishing the Role of CD44 and HA in HA-NW Binding with CD44-Expressing Cells

To investigate the role of CD44 for binding and uptake of HA-NWs, SKOV-3 cells were incubated with anti-CD44 antibody [MEM-85] (10 $\mu$L/ml) for 1 h, then the medium was removed, and the cells were washed by PBS buffer. Next, the medium containing HA-NWs (100 $\mu$g/mL) was added and allowed to incubate for 45 min. Finally, cells were washed with PBS buffer five times and collected for ICP analysis. Mouse IgG2b [PLPV219] (20 $\mu$L/$10^6$ cells) was used as an isotype control Ab for this experiment.

To investigate the role of HA for binding of HA-NWs, SKOV-3 cells ($1.2 \times 10^6$ cells per well) were incubated with free HA (10 mg/mL) for 0.5 h, and then the medium containing HA-NWs (100 $\mu$g/mL) was added and allowed to incubate for 1 h. Finally, cells were washed with PBS buffer five times and collected for ICP analysis to quantify Fe content.

### Energy-Dependent uptake of HA-NWs

To investigate the dependency of HA-NW uptake on energy, binding experiments were performed at 4 and 37 °C, respectively. SKOV-3 cells were cultured in a six-well plate ($3 \times 10^5$ cells/well) and incubated at 37 °C and 5% $CO_2$ until the cells became confluent. Cells were washed with PBS, and then FITC-HA-NWs (100 $\mu$g/mL) were dispersed in serum-free DMEM, added to the cells, and incubated for 1 h at 37 or 4 °C. Then the medium was removed, and the cells were washed with PBS three times. Next, the cells were detached by addition of trypsin, and they were neutralized by addition of 5 volumes of serum-containing DMEM. Finally, the cells were collected by centrifugation (1600 rpm, 5 min), resuspended in DMEM, transferred to a FACS tube, and kept on ice until FACS analysis.

### Analysis of RAW 264.7 Cell Inflammatory Responses to HA-NWs

Real-time PCR was used to measure inflammatory gene expression after treatment of mouse macrophage cells (RAW 264.7) with nanoparticles. Cells ($2 \times 10^5$/well) were cultured in a six-well plate overnight until they reached to 70–80% confluence. HA-NWs and HA-SPIONs (6 $\mu$g Fe/mL) were dispersed in serum-free medium and incubated with cells for 24 h. The medium was then removed, and cells were washed with PBS buffer twice. Next, the total RNA content of each well was extracted using an RNA extraction kit (RNeasy Mini Kit). Then extracted RNA was purified using a TURBO DNA-free Kit, and the obtained RNA was quantified by NanoDrop and stored at −80 °C. cDNA was prepared from RNA and used for real time PCR. All of the primers (Table 1) were ordered from IDT Co.

### Inflammatory Response to HA-NWs and HA-SPIONs in Vivo

The inflammatory responses to HA-NWs and HA-SPIONs in vivo were evaluated in wild-type mice. First, blood (200 $\mu$L) was collected through the saphenous vein to quantify the baseline levels of TNF$\alpha$ and IL-1$\beta$ for each mouse. Then, HA-NWs or HA-SPIONs (8 mg Fe/kg) were administered to each group through retro-orbital injection, and mice were sacrificed 1 and 24 h after injection and blood was collected through cardiac puncture. The blood was centrifuged (4000 rpm, 30 min), and serum was collected and stored at −20 °C. For the control study, PBS (100 $\mu$L) was administered. The amounts of TNF$\alpha$ and IL-1$\beta$ were quantified using a TNF$\alpha$ mouse ELISA kit and an IL-1$\beta$ mouse ELISA kit according to manufacturer's instructions.

### Cell Viability Assay of HA-NWs

EA.hy926 cells were cultured in a 96-well plate in DMEM cell culture media containing FBS (10%) for 24 h at 37 °C and 5% $CO_2$. The cells were then treated with different concentrations of NPs (0.0625, 0.125, 0.25, 0.5, 1 mg/mL) in serum-free medium. After 4 h of incubation at 37 °C, the medium was replaced with MTS solution (20 $\mu$L in 200 $\mu$L) in culture medium and incubated for 1 h at 37 °C. The developed brown color in the wells was an indication of live cells. The absorption of the plate was measured at 490 nm in an iMark microplate reader (BioRad). Wells without cells (blanks) were subtracted as background from each sample.

### Evaluation of the Biocompatibility of HA-NWs in Vivo

HA-NWs (8 mg Fe/kg) were administered to wild-type mice via retro-orbital injection. After 24 h, mouse blood was collected by cardiac puncture. Blood was stored in heparinized tubes (BD Vacutainer) at 4 °C and subsequently submitted for blood chemistry panel analysis. Moreover, liver, lung, and kidney were extracted and fixed in 10% buffered formalin solution for histopathological analysis. In addition, another group of mice received PBS injection as control for blood chemistry panel and histopathological analysis.

### In Vivo Imaging

Mice were purchased from Jackson Laboratories and were kept in the University Laboratory Animal Resources Facility of Michigan State University. All of the experimental procedures and guidelines for animal study were performed under approval of Institutional Animal Care and Use Committee (IACUC) of Michigan State University.

Six-week-old ApoE knockout mice were fed a high fat Western diet (TD.88137, Harlan Laboratories) for 8 weeks. The mice were scanned on 7T MRI before and after retro-orbital injections of NPs. The abdominal aorta was serially scanned until the aortic lumen signal intensities returned to the preinjection value. For control, HA-NWs were injected into age- and sex- matched wild type mice following an identical imaging protocol as performed on ApoE knockout mice. Moreover, to investigate the role of HA in mediating the selective binding of HA-NWs with CD44 on atherosclerotic plaques in vivo, bare NWs without HA were administered to ApoE knockout mice and MRI experiments were performed. For competition experiments, free HAs (33 mg/kg) were mixed with HA-NWs (8 mg Fe/kg) and then injected into ApoE knockout mice, and MRI images were collected.

Magnetic resonance experiments were performed on all mice anesthetized by 1.5% isoflurane following an induction using 4% isoflurane. Animals were secured in the supine position and restrained to reduce imaging artifacts due to motion. A Bruker 4-channel surface array was placed beneath the mouse to image the upper portion of abdominal aorta then placed in the isocenter of a Bruker 70/30 7 T horizontal bore imaging spectrometer. Serial images were acquired using the following acquisition parameters: TE/TR = 8/174 ms, in-plane resolution = 0.1 × 0.1 $mm^2$, slice thickness = 0.8 mm, Flip Angle = 50 deg, Number of Acquisition (NA) = 16. The TE and NA were selected to obtain good imaging contrast within a reasonable amount of time, i.e. around 5.9 min per acquisition.

### Histological Studies

ApoE knockout and wild-type control mice were sacrificed 2 h after administration of HA-NWs and the aortas were harvested. The abdominal aorta was cut and placed in sucrose solution (30%) overnight and then fixed using a freshly prepared formalin solution. Specimens were processed, embedded in paraffin, and sectioned on a rotary microtome at 4 $\mu$m. Sections were placed on slides and dried at 56 °C overnight. The slides were subsequently deparaffinized in xylene and hydrated through descending grades of ethyl alcohol to distilled water. Slides were placed in Tris-buffered saline pH 7.4 (Scytek Laboratories, Logan, UT) for 5 min for pH adjustment. Slides then underwent enzyme induced epitope retrieval using 2% proteinase K in TE buffer, pH 8.0 for 3 min at room temperature (Table 2), followed by rinses in several changes of distilled water. Endogenous peroxidases were blocked utilizing 3% hydrogen peroxide/methanol bath for 30 min followed by running tap and distilled water rinses. Following pretreatments, standard micropolymer complex staining steps were performed at room temperature on the IntelliPath Flex Autostainer. All staining steps were followed by rinses in TBS Autowash buffer (Biocare Medical, Concord, CA). After blocking for nonspecific protein with Mouse Block (Biocare) for 5 min, sections were incubated with specific primary antibodies (Table 2) in normal antibody diluent (NAD-Scytek) for 60 min. Micropolymer (Biocare) reagents were subsequently applied for specified incubations followed by reaction with Romulin AEC (Biocare) and counterstained with Cat Hematoxylin (Table 2).

In addition, ApoE knockout mouse aorta was incubated with HA-NWs (0.2 mg Fe/ml) at 37 °C for 1 h. Aorta tissues were then washed with PBS buffer for 5 times and immersed in freshly prepared mixture (1:1) of 2% HCl and an aqueous 2% potassium ferrocyanide solution for 15 min. The solution was removed and the tissues were washed with PBS buffer and stored in ethanol solution.

## RESULTS

### Synthesis and Characterization of HA-NWs

Synthesis of HA-NWs started from dextran-coated superparamagnetic iron oxide nanoworms (NWs), which were prepared through the coprecipitation of $Fe^{2+}$ and $Fe^{3+}$ ions in the presence of dextran (40 kDa).[22] Amine groups were introduced onto NWs by first cross-linking the surface dextran with epichlorohydrin followed by treatment with ammonia. HA was then conjugated onto aminated NWs through 2-chloro-4,6-dimethoxy-1,3,5-triazine

(CDMT) mediated amide bond formation[18] leading to HA-NWs (Figure 1a). The morphology of HA-NWs was characterized through TEM, which showed elongated worm like shape of the HA-NWs. The average length of HA-NW core is 65 ± 15 nm, corresponding to 10–20 NPs forming a single chain for each NW (Figure 1b). For comparison, the spherical shaped SPIONs with dextran coating were synthesized following a previously established procedure using dextran with average molecular weight of 10 kDa.[18] Subsequent introduction of HA onto SPIONs produced HA-SPIONs. TEM showed the spherical shape of HA-SPION with the average diameter of iron oxide core of 6 nm (Figure 1c). The key parameter in determining shape of the nanoconstruct is the molecular weight of dextran. Presumably, in the presence of higher molecular weight (40 kDa) of dextran during NW formation, the dextran coating on NPs linked multiple NPs forming a worm like structure.

The NW surface modification processes leading to HA-NWs were conveniently monitored by zeta potential analysis. The zeta potential value of as synthesized NWs is −6.0 mV in PBS buffer. Upon amination, the zeta potential became +4.5 mV due to the introduction of positively charged ammonium ions on the surface. The introduction of negatively charged HA onto aminated NWs decreased the zeta potential to −16 mV suggesting the successful conjugation of HA. The zeta potential of the corresponding HA-SPIONs was −14 mV, similar to that of HA-NWs. The hydrodynamic diameter of the HA-NW was 127 nm, increased from 93 nm for unmodified NWs. To facilitate tracking of the nanoprobes, FITC was introduced onto HA-NWs and HA-SPIONs producing FITC-HA-NWs and FITC-HA-SPIONs. The r2* magnetic relaxivity of HA-NWs was determined to be 110 (sec mMFe)$^{-1}$ at 7 T and while the r2* value was 52 (sec mMFe)$^{-1}$ for the corresponding HA-SPIONs. The high $r_2$* value suggests HA-NWs are good MR contrast agents (Figure S1).

For biological applications of HA-NWs, it is important to ensure that all HA in a sample of HA-NWs is conjugated with NWs, as residual free HA can potentially compete with HA-NWs for binding with CD44. To test this, we developed a new gel electrophoresis assay. Free HA, HA-SPION and HA-NW were electrophoresed on an agarose gel (0.8%) and stained with the Stains-All dye to visualize HA. Despite extensive washing after reaction of HA with aminated SPION or NW, there were still significant amounts of free HA associated with the particles (Figure S2a), presumably due to electrostatic interactions of HA with the particles. After investigating multiple methods, we found that washing the HA-SPION samples with 10% ammonium sulfate followed by ultrafiltration through centrifugal filters (MWCO 100 kDa), free HA can be successfully removed as confirmed by gel electrophoresis. HA-NWs required higher concentrations of ammonium sulfate (35%) to completely remove free HA possibly because of the stronger attraction of free HA with the longer NWs (Figure S2b). HA-NWs contaminated with free HA showed reduced binding with CD44-expressing cells, confirming the importance of completely removing free HA (Figure S3). TGA analysis showed that for purified HA-NWs, the organic content accounted for 91% of the total weight, with 70% coming from HA (Figure S4).

## Cellular Uptake of HA-NWs by CD44-Expressing Cells Is Much Higher than That of HA-SPIONs

With HA-SPIONs and HA-NWs in hand, their interactions with CD44-expressing vascular endothelial cells EA.hy926 (Figure S5), macrophage RAW264.7 cells,[24,25] and SKOV-3 cancer cells[26] were examined. FITC-labeled HA-NWs and HA-SPIONs were incubated with cells at equal initial FITC emission intensities, which was followed by extensive wash to remove unbound particles. The cells were then imaged through confocal microscopy. As shown in Figure 2b, f, both HA-NWs and HA-SPIONs could be found inside cells as indicated by the intracellular green fluorescence upon incubation. There was extensive colocalization of the FITC green fluorescence with the red fluorescence color from lysotracker indicating the nanoprobes entered lysosomes of the cells (Figure 2d, h). Cells treated with FITC-HA-NWs gave stronger FITC fluorescence intensities suggesting the uptake of HA-NWs was higher than that of HA-SPIONs (Figure 2b vs 2f).

To better quantify cellular uptake, flow cytometry analysis was performed, which showed cells incubated with FITC-HA-NWs gave more than four times higher fluorescence than those treated with FITC-HA-SPIONs (Figure 3a). To further confirm higher cellular uptake of HA-NWs, the amounts of iron inside cells were quantified by ICP-AES, which indicated significantly more iron in cells treated with HA-NWs than those with HA-SPIONs (Figure 3b).

## Both CD44 and HA Are Important for HA-NW Interactions with Cells

To confirm CD44 dependence of cellular interactions with HA-NWs, anti-CD44 monoclonal antibody (mAb) MEM-85 (IgG2b subtype) was added during cellular incubation of HA-NWs. MEM-85 is known to bind with CD44 and competitively block its interactions with HA.[27] ICP-AES quantification showed that MEM-85 led to 50% reduction of the intracellular level of iron, indicating that HA-NW uptake at least partially goes through CD44. A mouse IgG2b (PLPV219) not capable of binding CD44 was used as the isotype control mAb and intracellular iron quantification did not show reduction of HA-NW uptake when cells were coincubated with PLPV219 and HA-NWs (Figure 4).

The cellular uptakes of HA-NWs were measured under variable conditions including changes in temperature, incubation time, and incubation concentration. When cells were incubated with HA-NWs at 4 °C, HA-NW uptakes were much lower than those at 37 °C, indicating the uptake process was energy dependent (Figure S6).[28] Incubation of HA-NWs with cells at various time intervals showed that the uptake reached the maximum levels after 2 h of incubation (Figure S7). Treatment of cells with varying amounts of HA-NWs revealed that cellular uptake of HA-NWs could be saturated above 200 $\mu$g Fe/mL (Figure S8). These results are consistent with the idea that HA-NWs interact with cells through CD44 mediated endocytosis.

The importance of HA for cellular uptake was demonstrated by several experiments. Incubation of cells with FITC-labeled NWs without HA (FITC-NWs) showed little cellular uptake or binding when analyzed by FACS (Figure 5a). Treatment of cells with free HA (10 mg/mL) before addition of HA-NWs competitively inhibited cellular uptake of HA-NWs

(Figure 5b). Calculations showed that 140 times higher amount of free HA was needed to reduce the binding of HA-NW by 90% indicating the multivalent properties of HA-NWs leading to higher avidity binding between CD44 and HA.

## HA-NW Induced Much Lower Inflammatory Response than HA-SPIONs to Macrophages

For in vivo applications of nanoprobes, it is important that the probes are highly biocompatible. HA-NWs and HA-SPIONs were incubated with CD44 expressing mouse macrophage RAW264.7 cells,[24,25] and the levels of proinflammatory cytokines induced were quantified by real-time polymerase chain reaction (RT-PCR). Cytokines such as IL-1$\alpha$, IL-1$\beta$,[29,30] TNF$\alpha$,[31–33] and MCP-1 are inflammatory, which increases vascular permeability[34,35] and recruits inflammatory cells to plaques.[36] Spp can induce migration of macrophages to the sites of inflammation.[37] As shown in Figure 6, the levels of IL-1$\alpha$ expression in macrophages incubated with HA-NWs were less than 5% of those incubated with HA-SPIONs. In addition, cells treated with HA-NWs had significantly lower levels of other cytokines tested including IL-1$\beta$, MCP-1, TNF-$\alpha$, and Spp (Figure 6a). In addition, inflammatory responses to HA-NWs vs HA-SPIONS were evaluated in vivo by examining TNF$\alpha$ and IL-1$\beta$ levels in mouse blood 1 and 24 h after injection. Although TNF$\alpha$ level was not detectable in the blood before injection of HA nanoparticles, it increased 1 h following injection, and the TNF$\alpha$ level was 10 times higher in mice receiving HA-SPIONs vs those administered with HA-NWs indicating higher inflammatory responses to HA-SPIONs (Figure 6b). The TNF$\alpha$ level was not detectable 24 h after injection of both HA nanoparticles possibly due to feedback mechanisms that decrease TNF$\alpha$ production. IL-1$\beta$ was not detectable in mice blood before injection, 1 and 24 h after injection of HA nanoparticles (data not shown). Collectively, these results suggest higher biocompatibilities of HA-NWs compared to HA-SPIONs.

## HA-NWs Were Nontoxic to Cells and to Mice at the Concentrations Used for Imaging

To further test the biocompatibility of HA-NWs, cell viability assay was performed. Vascular endothelial EA.hy926 cells were incubated with HA-NWs and cell viabilities were determined by the MTS assay. No detrimental effects on cell viability were observed following incubation of HA-NWs up to 1 mg/mL (Figure S17).

To evaluate their biocompatibility in vivo, HA-NWs were injected into mice. One day after injection, blood was drawn from mice and a complete comprehensive blood chemistry panel analysis was performed. All of the parameters evaluated were in the normal range (Table S1). Most noteworthy were the negligible changes in alkaline phosphatase, aspartate aminotransferase, alanine transaminase, and $\gamma$-glutamyl transferase levels (markers for liver function) and total protein concentration (globulin and albumin) together with bilirubin level suggesting negligible acute toxicities. In addition, histopathological analysis did not show any signs of toxicity on liver, lung or kidney after HA-NW administration (Figure 7).

## HA-NWs Enabled in Vivo Imaging of Atherosclerosis Plaques in ApoE Knockout Mice

With the strong binding of HA-NWs to CD44-expressing cells and their biocompatibility demonstrated, we examined next the utility of HA-NWs for atherosclerotic plaque detection in ApoE knockout mice. Compared to the rabbit model which utilizes balloon catheter de-

endothelization surgical procedure of rabbit aorta to induce injury and initiate atherosclerosis development,[38] ApoE knockout mice are attractive as they closely mimic human conditions by spontaneously developing human like atherosclerotic plaques without the need for surgery.[39,40]

ApoE knockout mice were injected with HA-NWs retro-orbitally, and the mice were subjected to serial MRI using a T2* weighted imaging protocol focusing on the abdominal aorta area. Upon administration of HA-NWs (8 mg Fe/kg body weight), the image intensities of the lumen significantly decreased due to the loss of signals induced by HA-NWs (Figure 8). The lumen signal levels returned to preinjection levels within 80 min suggesting the majority of HA-NWs were cleared from the blood pool by that time. On aorta walls, the signal intensities of selective areas decreased to 20% of preinjection levels 20 min after injection presumably due to binding of HA-NWs and these signal intensities remained at ~20% of preinjection levels for more than 120 min (Figure 8). The signal changes could be observed in multiple locations of the aorta of ApoE knockout mice and the signals of the vessel walls fully recovered after 1 week (Figures S9–S12). Furthermore, even with a low dose of 2.8 mg Fe/kg of HA-NWs, effective plaque imaging could still be achieved (Figure S10).

To ascertain if signal changes were caused by HA-NW binding to atherosclerotic plaques in ApoE knockout mice, several control imaging experiments were performed. Following identical protocol as HA-NWs, NWs without HA were injected into ApoE knockout mice at the same Fe concentration and T2* weighted MRI were performed. No signal losses were observed from aorta wall of these mice (Figure S13b). In addition, when free HA was coinjected with HA-NWs to ApoE knockout mice, little signal changes were found from aorta walls possibly because free HA competed with HA-NWs for binding with CD44 rich plaques (Figure S13c). These results confirmed the importance of HA for plaque detection in vivo.

Another control experiment was performed by administering HA-NWs to wild type mice followed by MRI (Figure S13a). These mice did not have atherosclerosis, and their aorta walls did not exhibit significant changes in T2* weighted MRI after HA-NW injection. This suggests signal changes found in ApoE knockout mice caused by HA-NWs were not due to nonspecific binding of HA-NWs to mouse aorta walls.

The performance of HA-NWs in MRI of plaques was compared to HA-SPIONs next. HA-SPIONs (8 mg Fe/kg) were injected to ApoE knockout mice and their aortae were scanned following the identical T2* weighted MRI protocols as those receiving HA-NWs discussed above. As expected, upon HA-SPION administration, the lumen of aorta turned black in T2*-weighted images suggesting HA-SPIONs entered the blood causing significant MR signal losses (Figures S14 and S15). The signal intensities of lumen in these mice did not recover even 140 min after injection, which prevented the detection of plaques on aorta walls due to a lack of MR contrasts between the lumen and aorta walls. This was a stark difference from mice receiving HA-NWs (Figures 8 and S14), where lumen signals returned to preinjection levels within 80 min after injection presumably due to higher cellular uptake of

HA-NWs compared to HA-SPIONs. These results indicate that HA-NWs are not only more biocompatible but also more superior imaging agents than HA-SPIONs.

### Histological Analysis

F4/80 staining of abdominal aorta in ApoE knockout mouse showed accumulation of macrophages in abdominal aorta wall at the same locations where MRI signal changes were observed (Figures 9a, b). The same stain did not show macrophages accumulation in the wild type control mouse aorta (Figures 9c, d). Prussian blue staining of ApoE knockout mouse aorta after incubation with HA-NWs showed the presence of iron in lumen wall indicating binding of HA-NWs with CD44-expressing cells present in lumen wall (Figure 9e vs 9f). In addition, aorta tissues incubated with HA-NWs displayed more intense Prussian blue staining than those with HA-SPIONs (Figure S16), which was consistent with in vitro cellular studies suggesting stronger binding of HA-NW with plaque residing cells.

## DISCUSSION

SPIONs have been generally considered biocompatible.[41,42] However, they can impair iron homeostasis in cells, resulting in inflammation or other adverse effects.[43,44] While HA can reduce inflammatory activities, to further enhance the biocompatibilities and cellular binding, we have synthesized HA-NWs, which have elongated shape vs the spherical HA-SPIONs.

The size and shape of nanomaterials can impact cellular uptake and inflammatory responses.[45–47] Chen and co-workers synthesized polymer nanoparticles with either spherical or cylindrical shapes, which were then functionalized with mannose to yield glyconanoparticles.[48] Cellular uptake experiments with RAW 264.7 cells showed that spherical glyconanoparticles were taken up much more than cylindrical particles. The longer cylindrical glyconanoparticles induced higher inflammatory responses (IL-6) than shorter or spherical ones. The Chan group found that Hela cells internalized more spherical gold nanoparticles (AuNPs) than rod-shaped AuNPs.[49] Smaller spherical polymeric micelles were taken up by cells more than analogous cylindrical micelles.[50] Thiolated poly(methacrylic acid) capsules with different morphologies could influence cytokine secretion by macrophages: short rod-shaped capsules stimulated the generation of higher levels of TNF-$\alpha$ and IL-8 compared with spherical or long rod-shaped capsules.[51]

In contrast, a series of other studies showed higher uptake of rod like particles vs spherical ones. Sailor group demonstrated that NWs coated with tumor targeting peptide accumulated in tumor tissues in vivo twice as much as the spherical particles bearing the same ligand.[22,52] When spherical Au-NPs and Au nanorods coated with West Nile virus envelope were incubated with cells, 6 times more nanorods were found internalized than the corresponding spherical Au NPs.[53] Yet, the Au-NPs induced higher amounts of inflammatory cytokines such as TNF-$\alpha$ compared to the nanorods. The divergent impact of size and shape on cellular interactions could be affected by factors including (1) pathways for endocytosis;[48] (2) shape-dependent membrane wrapping time required to engulf the nanomaterials;[50] and (3) receptor density and rates of receptor endocytosis.

In our studies, despite similar surface charges, HA-NWs induced much lower inflammatory response compared to spherical HA-SPIONs, while the cellular uptake of HA-NWs was significantly higher (Figures 2,3, and 6). HA-NWs interacted with CD44-expressing cells in a CD44- and HA-dependent fashion as demonstrated in anti-CD44 mAb blocking and HA competition experiments (Figures 4 and 5). The higher cellular uptake of HA-NWs can be explained by molecular weight dependence of HA-CD44 interactions. HA exists in nature as a homopolymer of disaccharides of D-glucuronic acid $\beta$-1,4 linked with D-glucosamine. While CD44 can bind with HA as short as a hexasaccharide, the binding affinity can significantly increase with higher molecular weight of HA.[54–56] The NWs can provide a multivalent platform to present a large number of HA molecules on the surface leading to high avidity with the CD44 receptor. This is supported by our observation that 140 times more free HA is needed to reduce the binding of HA-NW by 90% (Figure 5). Compared to the corresponding HA-SPIONs, HA-NWs have elongated shapes. As a result, one HA-NW can possibly simultaneously engage a larger number of CD44 receptors on cell surface leading to stronger binding to cells.

The biological activities of HA are dependent upon its molecular weight.[57] Low molecular weight HAs can be inflammatory, while the high molecular weight HAs (million Daltons) are anti-inflammatory.[57] As one NW consists of multiple SPIONs and contains more HA per particle, it is possible that HA-NWs can better mimic high molecular weight HA, more effectively reducing the inflammatory activities resulting from the iron oxide core of the nanoprobes.

Due to the severe adverse effects of atherosclerosis on public health, there is high interest in developing imaging methods to detect atherosclerotic plaques. MRI is a powerful technique for morphological imaging of blood vessels.[6,7] To better characterize plaques, contrast agents that can aid in the depiction of molecular process signatures other than plaque morphology are highly desired.[8,9] SPIONs are a popular class of contrast agents,[37,58] which lead to reduction of MR signals in T2 and T2* weighted images creating contrast from the surroundings. Earlier imaging studies using SPIONs take advantage of the nonspecific uptake of the NPs by macrophages.[59–62] As a result, high concentrations of SPIONs (typical dose 56 mg Fe/kg) need to be administered, which produce complete signal losses in lumen of the blood vessels.[59–63] In order to obtain sufficient contrast between plaques and lumen and allow sufficient clearance of NPs from the blood pool and the background, imaging was commonly performed at least 1 day and optimally 4 to 5 days after injection.[59–62,64] In addition, longitudinal monitoring of plaque development will require regular administration of the nanoprobes. The need for prolonged delay of MRI after probe administration coupled with the possible inflammatory activities of SPIONs raise cautions for wide applications of these particles.

To improve on the performance of SPIONs and to provide information on the molecular composition and/or the state of the plaque, various targeting ligands have been immobilized onto SPIONs,[65–69] which include peptide binders and mAbs for vascular cell adhesion molecule-1 (VCAM-1) and annexin V for apoptotic cells. Some of these probes have been employed to evaluate plaques in vivo. However, in many of these studies, high

concentrations of NPs and/or prolonged delay after injection were still necessary for imaging.

In our work, we selectively target CD44, which is a receptor highly expressed in multiple plaque residing cells including endothelial cells, macrophages, and monocytes.[10,12–14,70] A significant advantage using HA-NWs is that plaque detection and imaging can be performed right after probe injection. This is probably due to two reasons: (1) With the strong binding to CD44 and the high magnetic relaxivities of HA-NWs, relatively small amounts of HA-NW (2.8 mg Fe/kg) are needed to visualize the plaques in mice. As a result, the lumen of the blood vessels appeared gray rather than black in T2* weighted MRI, allowing the distinction between lumen and the black plaque site even right after injection. (2) Because CD44 is present on endothelial cells at the surface of the plaque tissues, HA-NW could rapidly bind with CD44 without the need to wait for particle penetrations into the tissues.

## CONCLUSION

We have synthesized HA-conjugated NWs for the first time. HA-NWs can interact more strongly than the corresponding spherical-shaped HA-SPIONs with CD44-expressing cells in CD44- and HA-dependent manners. Furthermore, the inflammatory activities were significantly attenuated in HA-NWs suggesting engineering of nanomaterial shape and morphology can be a promising future direction to develop probes for plaque detection. The high avidity to CD44, good biocompatibility, and high magnetic relaxivity of HA-NW render it an attractive probe for in vivo imaging and detection of atherosclerotic plaques as well as for longitudinal monitoring of plaques to aid in the development of novel therapeutic interventions.

## Supplementary Material

Refer to Web version on PubMed Central for supplementary material.

## Acknowledgments

We are grateful for the financial support from the National Institute of General Medical Sciences, NIH (R01GM072667), and Michigan State University toward this project. We thank the Department of Radiology, Michigan State University, for generously providing MRI scanner time.

## References

1. Weber C, Noels H. Atherosclerosis: current pathogenesis and therapeutic options. Nat Med. 2011; 17:1410–1422. [PubMed: 22064431]
2. Chelly J, Mongardon N, Dumas F, Varenne O, Spaulding C, Vignaux O, Carli P, Charpentier J, Pène F, Chiche JD, Mira JP, Cariou A. Benefit of an early and systematic imaging procedure after cardiac arrest: insights from the PROCAT (Parisian Region Out of Hospital Cardiac Arrest) registry. Resuscitation. 2012; 83:1444–1450. [PubMed: 22922264]
3. Benjamin EJ, Blaha MJ, Chiuve SE, Cushman M, Das SR, Deo R, de Ferranti SD, Floyd J, Fornage M, Gillespie C, Isasi CR, Jiménez MC, Jordan LC, Judd SE, Lackland D, Lichtman JH, Lisabeth L, Liu S, Longenecker CT, Mackey RH, Matsushita K, Mozaffarian D, Mussolino ME, Nasir K, Neumar RW, Palaniappan L, Pandey DK, Thiagarajan RR, Reeves MJ, Ritchey M, Rodriguez CJ, Roth GA, Rosamond WD, Sasson C, Towfighi A, Tsao CW, Turner MB, Virani SS, Voeks JH, Willey JZ, Wilkins JT, Wu JH, Alger HM, Wong SS, Muntner P. Heart disease and stroke statistics

—2017 update: a report from the American heart association. Circulation. 2017; 135:e146. [PubMed: 28122885]

4. Tarkin JM, Dweck MR, Evans NR, Takx RAP, Brown AJ, Tawakol A, Fayad ZA, Rudd JHF. Imaging atherosclerosis. Circ Res. 2016; 118:750–769. [PubMed: 26892971]
5. Mulder WJM, Jaffer FA, Fayad ZA, Nahrendorf M. Imaging and nanomedicine in inflammatory atherosclerosis. Sci Transl Med. 2014; 6:239sr1. [PubMed: 24898749]
6. Moonen, RPM., Strijkers, GJ., Fayad, ZA., Daemen, MJAP., Nicolay, K. Molecular MR Imaging of Atherosclerosis. In: Aikawa, E., editor. Cardiovascular imaging: arterial and aortic valve inflammation and calcification. Springer International Publishing; Cham: 2015. p. 269-296.
7. Corti R, Fuster V. Imaging of atherosclerosis: magnetic resonance imaging. Eur Heart J. 2011; 32:1709–1719. [PubMed: 21508002]
8. Hyafil F, Feldman L, Fayad ZA, Le Guludec D. Imaging atherosclerotic plaques with MRI: role of contrast agents. Curr Cardiovasc Imaging Rep. 2013; 6:76–88.
9. Gao Z, Ma T, Zhao E, Docter D, Yang W, Stauber RH, Gao M. Small is smarter: nano MRI contrast agents – advantages and recent achievements. Small. 2016; 12:556–576. [PubMed: 26680328]
10. Zhao L, Lee E, Zukas AM, Middleton MK, Kinder M, Acharya PS, Hall JA, Rader DJ, Puré E. CD44 expressed on both bone marrow–derived and non–bone marrow–derived cells promotes atherogenesis in ApoE-deficient mice. Arterioscler, Thromb, Vasc Biol. 2008; 28:1283–1289. [PubMed: 18420998]
11. Puré E, Cuff CA. A crucial role for CD44 in inflammation. Trends Mol Med. 2001; 7:213–221. [PubMed: 11325633]
12. Cuff CA, Kothapalli D, Azonobi I, Chun S, Zhang Y, Belkin R, Yeh C, Secreto A, Assoian RK, Rader DJ, Puré E. The adhesion receptor CD44 promotes atherosclerosis by mediating inflammatory cell recruitment and vascular cell activation. J Clin Invest. 2001; 108:1031–1040. [PubMed: 11581304]
13. Hägg D, Sjöberg S, Hultén LM, Fagerberg B, Wiklund O, Rosengren A, Carlsson LMS, Borén J, Svensson PA, Krettek A. Augmented levels of CD44 in macrophages from atherosclerotic subjects: a possible IL-6–CD44 feedback loop? Atherosclerosis. 2007; 190:291–297. [PubMed: 16620830]
14. Kolodgie FD, Burke AP, Farb A, Weber DK, Kutys R, Wight TN, Virmani R. Differential accumulation of proteoglycans and hyaluronan in culprit lesions: insights into plaque erosion. Arterioscler, Thromb, Vasc Biol. 2002; 22:1642–1648. [PubMed: 12377743]
15. Misra S, Hascall VC, Markwald RR, Ghatak S. Interactions between hyaluronan and its receptors (CD44, RHAMM) regulate the activities of inflammation and cancer. Front Immunol. 2015; 6:201. [PubMed: 25999946]
16. Toole BP. Hyaluronan: from extracellular glue to pericellular cue. Nat Rev Cancer. 2004; 4:528–539. [PubMed: 15229478]
17. Maiti A, Maki G, Johnson P. TNF-alpha induction of CD44-mediated leukocyte adhesion by sulfation. Science. 1998; 282:941–943. [PubMed: 9794764]
18. Kamat M, El-boubbou K, Zhu DC, Lansdell T, Lu X, Li W, Huang X. Hyaluronic acid immobilized magnetic nanoparticles for active targeting and imaging of macrophages. Bioconjugate Chem. 2010; 21:2128–2135.
19. El-Dakdouki MH, El-Boubbou K, Kamat M, Huang R, Abela GS, Kiupel M, Zhu DC, Huang X. CD44 targeting magnetic glyconanoparticles for atherosclerotic plaque imaging. Pharm Res. 2014; 31:1426–1437. [PubMed: 23568520]
20. Lee GY, Kim JH, Choi KY, Yoon HY, Kim K, Kwon IC, Choi K, Lee BH, Park JH, Kim IS. Hyaluronic acid nanoparticles for active targeting atherosclerosis. Biomaterials. 2015; 53:341–348. [PubMed: 25890732]
21. Beldman TJ, Senders ML, Alaarg A, Pérez-Medina C, Tang J, Zhao Y, Fay F, Deichmöller J, Born B, Desclos E, van der Wel NN, Hoebe RA, Kohen F, Kartvelishvily E, Neeman M, Reiner T, Calcagno C, Fayad ZA, de Winther MPJ, Lutgens E, Mulder WJM, Kluza E. Hyaluronan nanoparticles selectively target plaque-associated macrophages and improve plaque stability in atherosclerosis. ACS Nano. 2017; 11:5785–5799. [PubMed: 28463501]

22. Park JH, von Maltzahn G, Zhang L, Schwartz MP, Ruoslahti E, Bhatia SN, Sailor MJ. Magnetic iron oxide nanoworms for tumor targeting and imaging. Adv Mater. 2008; 20:1630–1635. [PubMed: 21687830]
23. Lee HG, Cowman MK. An agarose gel electrophoretic method for analysis of hyaluronan molecular weight distribution. Anal Biochem. 1994; 219:278–287. [PubMed: 8080084]
24. Marroquin CE, Downey L, Guo H, Kuo PC. Osteopontin increases CD44 expression and cell adhesion in RAW 264.7 murine leukemia cells. Immunol Lett. 2004; 95:109–112. [PubMed: 15325806]
25. Amash A, Wang L, wang Y, Bhakta V, Fairn GD, Hou M, Peng J, Sheffield WP, Lazarus AH. CD44 antibody inhibition of macrophage phagocytosis targets Fc$\gamma$ receptor– and complement receptor 3–dependent mechanisms. J Immunol. 2016; 196:3331–3340. [PubMed: 26944929]
26. El-Dakdouki MH, Zhu DC, El-Boubbou K, Kamat M, Chen J, Li W, Huang X. Development of multifunctional hyaluronan-coated nanoparticles for imaging and drug delivery to cancer cells. Biomacromolecules. 2012; 13:1144–1151. [PubMed: 22372739]
27. Assmann V, Fieber C, Termeer CC, Herrlich P, Hofmann M, Simon JC, Ahrens T. CD44 is the principal mediator of hyaluronic-acid-induced melanoma cell proliferation. J Invest Dermatol. 2001; 116:93–101. [PubMed: 11168803]
28. Qhattal HSS, Liu X. Characterization of CD44-mediated cancer cell uptake and intracellular distribution of hyaluronan-grafted liposomes. Mol Pharmaceutics. 2011; 8:1233–1246.
29. Garlanda C, Dinarello CA, Mantovani A. The Interleukin-1 family: back to the future. Immunity. 2013; 39:1003–1018. [PubMed: 24332029]
30. Radhakrishnan G, Suzuki R, Maeda H, Yamamoto M, Hirose N, Gopalrao RK, Lee GH, Hayashi Y, Rao P, Sasaguri S. Inhibition of neointimal hyperplasia development by MCI-186 is correlated with downregulation of nuclear factor-kappaB pathway. Circ J. 2008; 72:800–806. [PubMed: 18441462]
31. Wolfs IM, Donners MM, de Winther MP. Differentiation factors and cytokines in the atherosclerotic plaque micro-environment as a trigger for macrophage polarisation. Thromb Haemostasis. 2011; 106:763–771. [PubMed: 21947328]
32. Petrache I, Birukova A, Ramirez SI, Garcia JG, Verin AD. The role of the microtubules in tumor necrosis factor-alpha-induced endothelial cell permeability. Am J Respir Cell Mol Biol. 2003; 28:574–581. [PubMed: 12707013]
33. Ohta H, Wada H, Niwa T, Kirii H, Iwamoto N, Fujii H, Saito K, Sekikawa K, Seishima M. Disruption of tumor necrosis factor-alpha gene diminishes the development of atherosclerosis in ApoE-deficient mice. Atherosclerosis. 2005; 180:11–17. [PubMed: 15823270]
34. Bai L, Li Z, Li Q, Guan H, Zhao S, Liu R, Wang R, Zhang J, Jia Y, Fan J, Wang N, Reddy JK, Shyy JYJ, Liu E. Mediator 1 is atherosclerosis protective by regulating macrophage polarization. Arterioscler, Thromb, Vasc Biol. 2017; 37:1470–1481. [PubMed: 28642237]
35. Kuwahara F, Kai H, Tokuda K, Shibata R, Kusaba K, Tahara N, Niiyama H, Nagata T, Imaizumi T. Hypoxia-inducible factor-1alpha/vascular endothelial growth factor pathway for adventitial vasa vasorum formation in hypertensive rat aorta. Hypertension. 2002; 39:46–50. [PubMed: 11799077]
36. Jaipersad AS, Lip GY, Silverman S, Shantsila E. The role of monocytes in angiogenesis and atherosclerosis. J Am Coll Cardiol. 2014; 63:1–11. [PubMed: 24140662]
37. Corot C, Robert P, Idée JM, Port M. Recent advances in iron oxide nanocrystal technology for medical imaging. Adv Drug Delivery Rev. 2006; 58:1471–1504.
38. Abela GS, Picon PD, Friedl SE, Gebara OC, Miyamoto A, Federman M, Tofler GH, Muller JE. Triggering of plaque disruption and arterial thrombosis in an atherosclerotic rabbit model. Circulation. 1995; 91:776–784. [PubMed: 7828306]
39. Rosenfeld ME, Polinsky P, Virmani R, Kauser K, Rubanyi G, Schwartz SM. Advanced atherosclerotic lesions in the innominate artery of the ApoE knockout mouse. Arterioscler, Thromb, Vasc Biol. 2000; 20:2587–2592. [PubMed: 11116057]
40. Wouters K, Shiri-Sverdlov R, van Gorp PJ, van Bilsen M, Hofker MH. Understanding hyperlipidemia and atherosclerosis: lessons from genetically modified apoe and ldlr mice. Clin Chem Lab Med. 2005; 43:470–479. [PubMed: 15899668]

41. Yu M, Huang S, Yu KJ, Clyne AM. Dextran and polymer polyethylene glycol (PEG) coating reduce both 5 and 30 nm iron oxide nanoparticle cytotoxicity in 2D and 3D cell culture. Int J Mol Sci. 2012; 13:5554–5570. [PubMed: 22754315]
42. Weissleder R, Stark DD, Engelstad BL, Bacon BR, Compton CC, White DL, Jacobs P, Lewis J. Superparamagnetic iron oxide: pharmacokinetics and toxicity. AJR, Am J Roentgenol. 1989; 152:167–173. [PubMed: 2783272]
43. Singh N, Jenkins GJS, Asadi R, Doak SH. Potential toxicity of superparamagnetic iron oxide nanoparticles (SPION). Nano Rev. 2010; 1:5358.
44. Berry CC, Wells S, Charles S, Aitchison G, Curtis ASG. Cell response to dextran-derivatised iron oxide nanoparticles post internalisation. Biomaterials. 2004; 25:5405–5413. [PubMed: 15130725]
45. Benne N, van Duijn J, Kuiper J, Jiskoot W, Slütter B. Orchestrating immune responses: how size, shape and rigidity affect the immunogenicity of particulate vaccines. J Controlled Release. 2016; 234:124–134.
46. Truong NP, Whittaker MR, Mak CW, Davis TP. The importance of nanoparticle shape in cancer drug delivery. Expert Opin Drug Delivery. 2015; 12:129–142.
47. Verma A, Stellacci F. Effect of surface properties on nanoparticle-cell interactions. Small. 2010; 6:12–21. [PubMed: 19844908]
48. Li Z, Sun L, Zhang Y, Dove AP, O'Reilly RK, Chen G. Shape effect of glyco-nanoparticles on macrophage cellular uptake and immune response. ACS Macro Lett. 2016; 5:1059–1064. [PubMed: 27695648]
49. Chithrani BD, Ghazani AA, Chan WCW. Determining the size and shape dependence of gold nanoparticle uptake into mammalian cells. Nano Lett. 2006; 6:662–668. [PubMed: 16608261]
50. Zhang K, Fang H, Chen Z, Taylor JSA, Wooley KL. Shape effects of nanoparticles conjugated with cell-penetrating peptides (HIV Tat PTD) on CHO cell uptake. Bioconjugate Chem. 2008; 19:1880–1887.
51. Chen X, Yan Y, Müllner M, Ping Y, Cui J, Kempe K, Cortez-Jugo C, Caruso F. Shape-dependent activation of cytokine secretion by polymer capsules in human monocyte-derived macrophages. Biomacromolecules. 2016; 17:1205–1212. [PubMed: 26919729]
52. Park JH, von Maltzahn G, Zhang L, Derfus AM, Simberg D, Harris TJ, Ruoslahti E, Bhatia SN, Sailor MJ. Systematic surface engineering of magnetic nanoworms for in vivo tumor targeting. Small. 2009; 5:694–700. [PubMed: 19263431]
53. Niikura K, Matsunaga T, Suzuki T, Kobayashi S, Yamaguchi H, Orba Y, Kawaguchi A, Hasegawa H, Kajino K, Ninomiya T, Ijiro K, Sawa H. Gold nanoparticles as a vaccine platform: influence of size and shape on immunological responses *in vitro* and *in vivo*. ACS Nano. 2013; 7:3926–3938. [PubMed: 23631767]
54. Tammi R, MacCallum D, Hascall VC, Pienimäki JP, Hyttinen M, Tammi M. Hyaluronan bound to CD44 on keratinocytes is displaced by hyaluronan decasaccharides and not hexasaccharides. J Biol Chem. 1998; 273:28878–28888. [PubMed: 9786890]
55. Banerji S, Wright AJ, Noble M, Mahoney DJ, Campbell ID, Day AJ, Jackson DG. Structures of the CD44–hyaluronan complex provide insight into a fundamental carbohydrate protein interaction. Nat Struct Mol Biol. 2007; 14:234–239. [PubMed: 17293874]
56. Mizrahy S, Raz SR, Hasgaard M, Liu H, Soffer-Tsur N, Cohen K, Dvash R, Landsman-Milo D, Bremer MGEG, Moghimi SM, Peer D. Hyaluronan-coated nanoparticles: the influence of the molecular weight on CD44-hyaluronan interactions and on the immune response. J Controlled Release. 2011; 156:231–238.
57. Jiang D, Liang J, Noble PW. Hyaluronan as an immune regulator in human diseases. Physiol Rev. 2011; 91:221–264. [PubMed: 21248167]
58. Thorek DLJ, Chen AK, Czupryna J, Tsourkas A. Superparamagnetic iron oxide nanoparticle probes for molecular imaging. Ann Biomed Eng. 2006; 34:23–38. [PubMed: 16496086]
59. Sigovan M, Boussel L, Sulaiman A, Sappey-Marinier D, Alsaid H, Desbleds-Mansard C, Ibarrola D, Gamondès D, Corot C, Lancelot E, Raynaud JS, Vives V, Laclédère C, Violas X, Douek PC, Canet-Soulas E. Rapid-clearance iron nanoparticles for inflammation imaging of atherosclerotic plaque: initial experience in animal model. Radiology. 2009; 252:401–409. [PubMed: 19703881]

60. Morris JB, Olzinski AR, Bernard RE, Aravindhan K, Mirabile RC, Boyce R, Willette RN, Jucker BM. p38 MAPK inhibition reduces aortic ultrasmall superparamagnetic iron oxide uptake in a mouse model of atherosclerosis MRI assessment. Arterioscler, Thromb, Vasc Biol. 2007; 28:265–271. [PubMed: 18162612]

61. Durand E, Raynaud JS, Bruneval P, Brigger I, Al Haj Zen A, Mandet C, Lancelot E, Lafont A. Magnetic resonance imaging of ruptured plaques in the rabbit with ultrasmall superparamagnetic particles of iron oxide. J Vasc Res. 2007; 44:119–128. [PubMed: 17215583]

62. Ruehm SG, Corot C, Vogt P, Kolb S, Debatin JF. Magnetic resonance imaging of atherosclerotic plaque with ultrasmall superparamagnetic particles of iron oxide in hyperlipidemic rabbits. Circulation. 2001; 103:415–422. [PubMed: 11157694]

63. Morishige K, Kacher DF, Libby P, Josephson L, Ganz P, Weissleder R, Aikawa M. High-resolution magnetic resonance imaging enhanced with superparamagnetic nanoparticles measures macrophage burden in atherosclerosis. Circulation. 2010; 122:1707–1715. [PubMed: 20937980]

64. Hyafil F, Laissy JP, Mazighi M, Tchétché D, Louedec L, Adle-Biassette H, Chillon S, Henin D, Jacob MP, Letourneur D, Feldman LJ. Ferumoxtran-10–enhanced MRI of the hypercholesterolemic rabbit aorta relationship between signal loss and macrophage infiltration. Arterioscler, Thromb, Vasc Biol. 2006; 26:176–181. [PubMed: 16269663]

65. McAteer MA, Schneider JE, Ali ZA, Warrick N, Bursill CA, von zur Muhlen C, Greaves DR, Neubauer S, Channon KM, Choudhury RP. Magnetic resonance imaging of endothelial adhesion molecules in mouse atherosclerosis using dual-targeted microparticles of iron oxide. Arterioscler, Thromb, Vasc Biol. 2007; 28:77–83. [PubMed: 17962629]

66. Smith BR, Heverhagen J, Knopp M, Schmalbrock P, Shapiro J, Shiomi M, Moldovan NI, Ferrari M, Lee SC. Localization to atherosclerotic plaque and biodistribution of biochemically derivatized superparamagnetic iron oxide nanoparticles (SPIONs) contrast particles for magnetic resonance imaging (MRI). Biomed Microdevices. 2007; 9:719–727. [PubMed: 17562181]

67. Nahrendorf M, Jaffer FA, Kelly KA, Sosnovik DE, Aikawa E, Libby P, Weissleder R. Noninvasive vascular cell adhesion molecule-1 imaging identifies inflammatory activation of cells in atherosclerosis. Circulation. 2006; 114:1504–1511. [PubMed: 17000904]

68. Tu C, Ng TSC, Sohi HK, Palko HA, House A, Jacobs RE, Louie AY. Receptor-targeted iron oxide nanoparticles for molecular MR imaging of inflamed atherosclerotic plaques. Biomaterials. 2011; 32:7209–7216. [PubMed: 21742374]

69. Meding J, Urich M, Licha K, Reinhardt M, Misselwitz B, Fayad ZA, Weinmann HJ. Magnetic resonance imaging of atherosclerosis by targeting extracellular matrix deposition with gadofluorine M. Contrast Media Mol Imaging. 2007; 2:120–129. [PubMed: 17557276]

70. Sadowitz B, Seymour K, Gahtan V, Maier KG. The role of hyaluronic acid in atherosclerosis and intimal hyperplasia. J Surg Res. 2012; 173:e63–e72. [PubMed: 22104612]

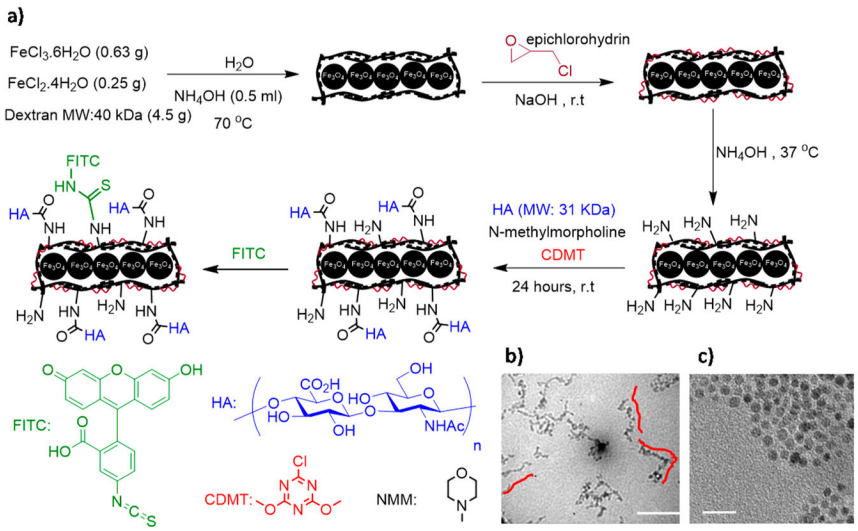


**Figure 1.**

(a) Synthesis of HA-NWs. (b) TEM images for HA-NWs showed the elongated shape of HA-NWs. Three representative worms were traced with red lines. (c) TEM image for HA-SPIONs showed spherical morphology. Scale bars are 50 and 20 nm for b and c, respectively.

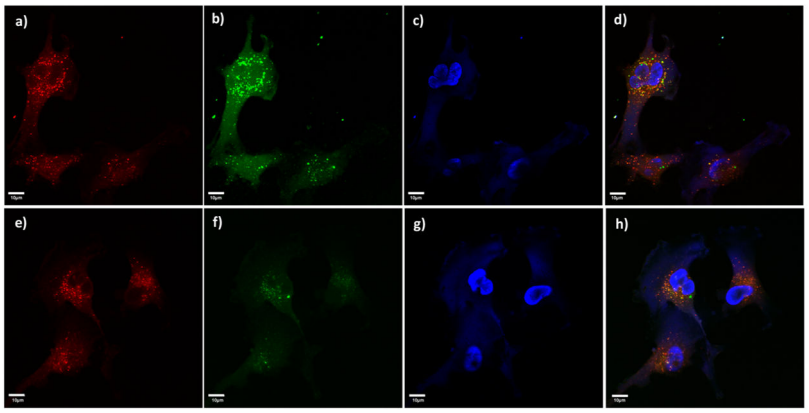


**Figure 2.**

Confocal microscopy showed stronger interaction for HA-NWs (a–d) than the corresponding HA-SPIONs (e–h) with CD44-expressing cells such as vascular endothelial cells EA.hy926: (a, e) red lysotracker channel showing locations of the lysosomes; (b, f) FITC channels showing locations of the nanoprobes; (c, g) DAPI channels showing location of nuclei; (d, h) overlays of red lysotracker and green FITC and DAPI channels. Scale bars are 10 $\mu$m.

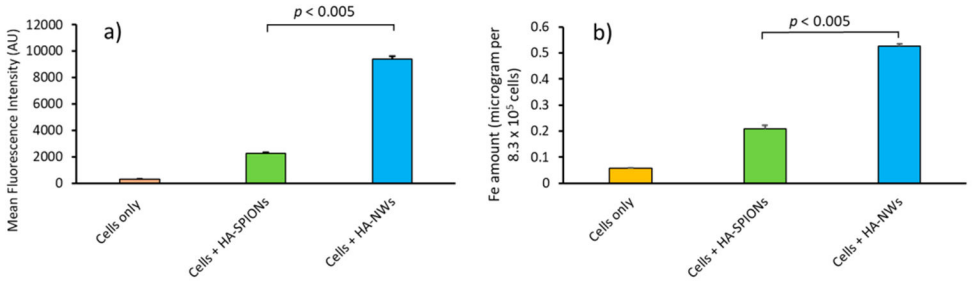


**Figure 3.**

HA-NW uptake by CD44 expressing EA.hy926 cells is higher than that of HA-SPIONs. (a) Mean fluorescence intensities of EA.hy926 cells following incubations with HA-NWs and HA-SPIONs. (b) Intracellular Fe content was quantified by ICP after incubations with HA-NWs and HA-SPIONs. The *p*-values were obtained from student's *t*-test.

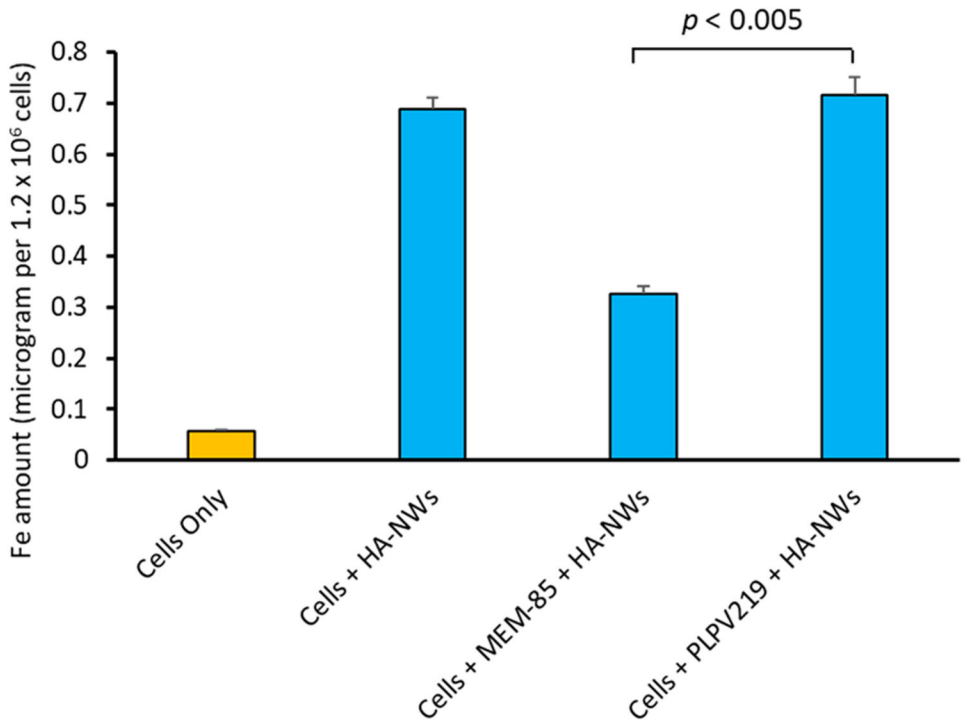


**Figure 4.**

Pretreatment of cells with an anti-CD44 mAb MEM-85 resulted in 50% reduction of HA-NW cellular uptake, while the non-CD44 binding isotype control mAb PLPV219 did not have much effects on cellular uptake of HA-NWs. The *p*-value was obtained from student's *t*-test.

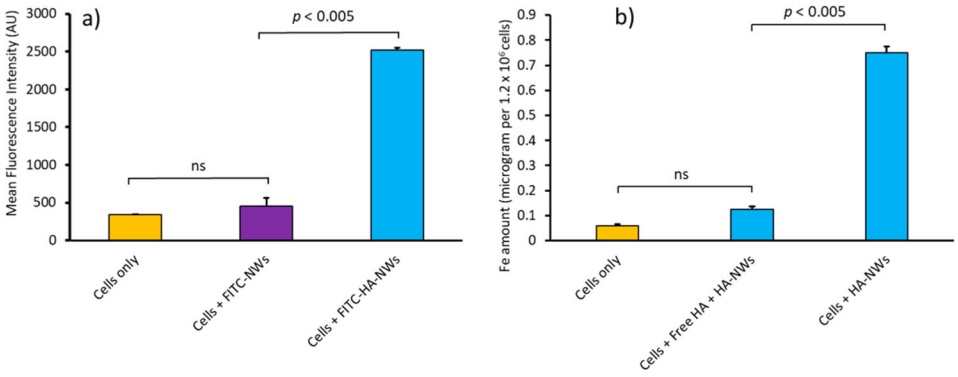


**Figure 5.**

Presence of HA on HA-NWs was necessary for their cellular interactions with cells: (a) cells were treated with equivalent amounts of NWs and HA-NWs and analyzed by FACS; (b) Pretreatment of cells with free HA significantly reduced cellular interactions with HA-NWs. The *p*-values were obtained from student's *t*-test.

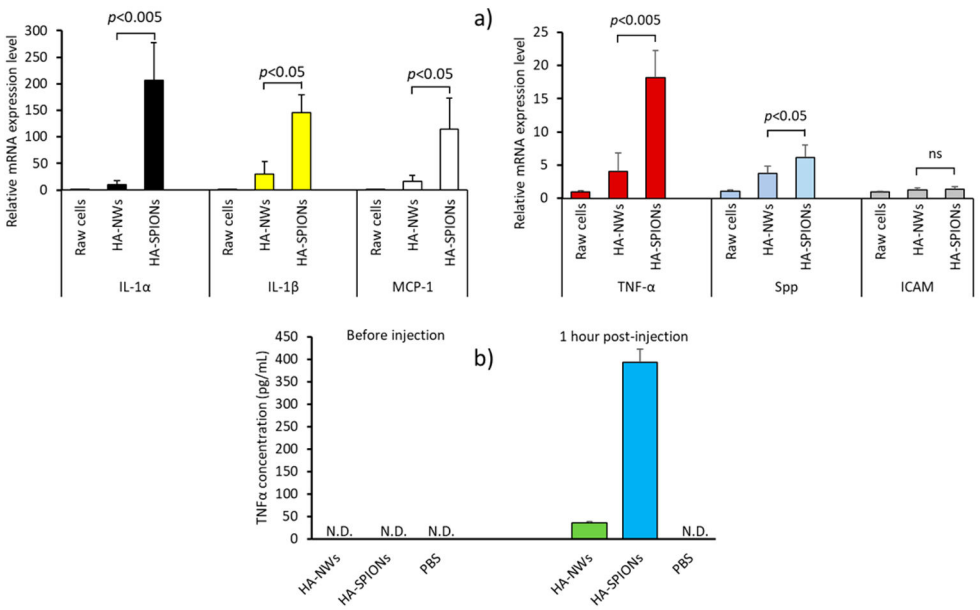


**Figure 6.**

Inflammatory response to HA nanoparticles. (a) Expression levels of inflammatory genes after treatments of RAW264.7 cells with equivalent amounts of HA-SPIONs and HA-NWs. HA-NWs induced significantly less inflammatory cytokines compared to HA-SPIONs. (b) TNF$\alpha$ levels in blood from mice before and after injection of HA nanoparticles. HA-SPIONs induced a higher level of TNF$\alpha$ 1 h after injection compared to HA-NWs. N.D.: not detected.

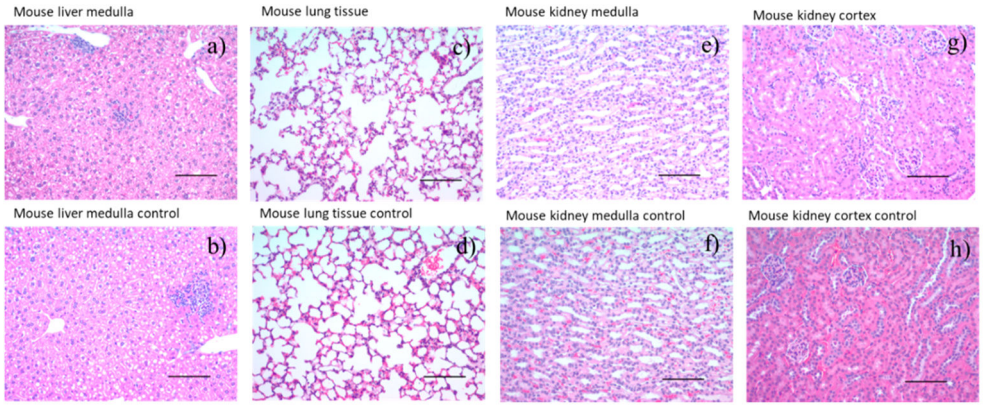


**Figure 7.**

Histopathology images of extracted organs 24 h after HA-NW administration. No significant differences were observed in these organs compared to those from control mice receiving PBS only: (a) mouse liver medulla, (c) mouse lung tissue, (e) mouse kidney medulla, and (g) mouse kidney cortex 24 h after HA-NW injection; (b) mouse liver medulla, (d) mouse lung tissue, (f) mouse kidney medulla, and (h) mouse kidney cortex images from control mouse. Scale bar is 100 $\mu$m.

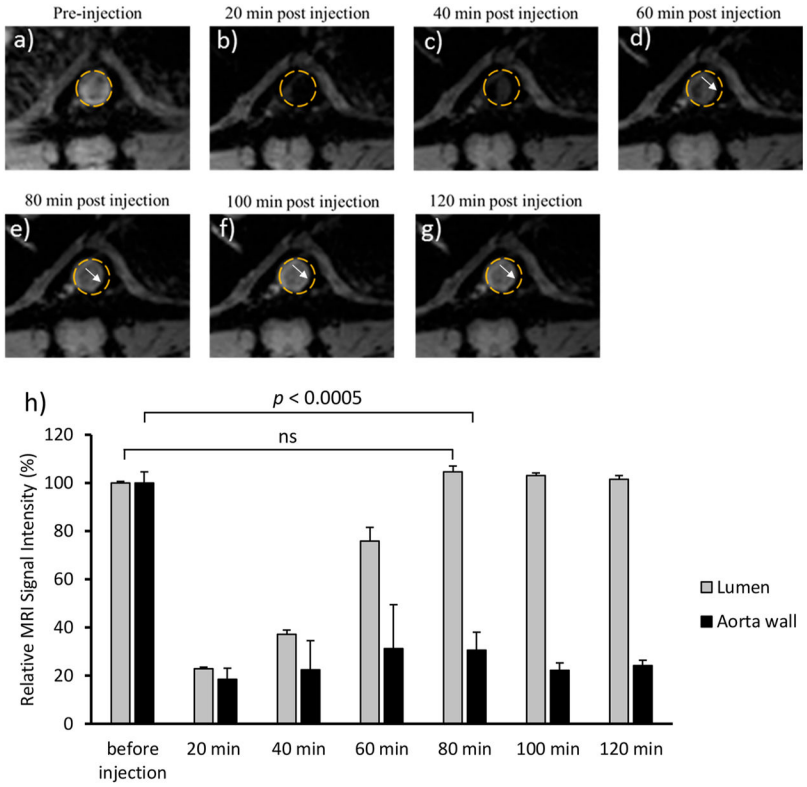


**Figure 8.**

T2*-weighted MR images of ApoE knockout mice aorta (a) before injection of HA-NWs (8 mg Fe/kg body weight) and different time intervals after injection of HA-NWs (b–g). Areas of the aorta walls that have undergone contrast changes are highlighted by white arrows. (h) Quantification of signal intensity changes for lumen and aorta wall before injection and at different time intervals after injection of HA-NWs. The *p*-value was obtained from student's *t* test.

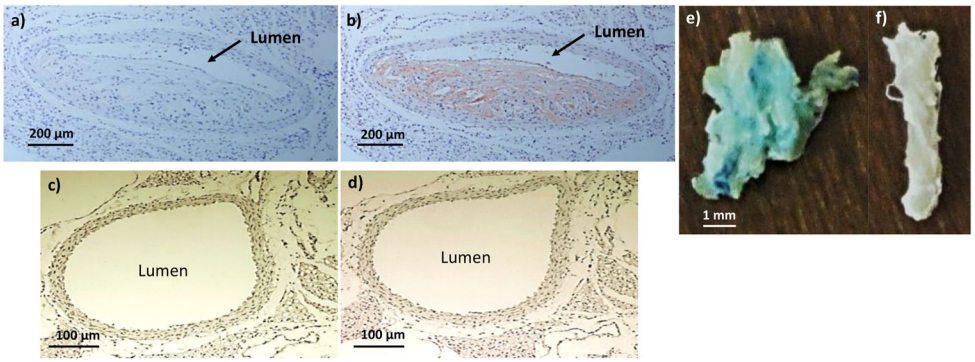


**Figure 9.**

F4/80 staining showed macrophage accumulation in ApoE knockout mouse aorta. (a, b) ApoE knockout mouse aorta slice before and after F4/80 staining. (c, d) Wild-type mouse aorta slice before and after F4/80 staining. Prussian blue staining of (e) ApoE knockout mouse and (f) wild type aorta after incubation with HA-NWs. The staining (blue green color) was much more intense in panel e than f.

**Table 1**

Primer Sequences of Inflammatory Genes Used for RT-PCR Study

| gene | forward primer (5′→3′) | reverse primer (5′→3′) |
|---|---|---|
| IL-la | CGAAGACTACAGTTCTGCCATT | GACGTTTCAGAGGTTCTCAGAG |
| IL-lb | TTCAGGCAGGCAGTATCACTC | GAAGGTCCACGGGAAAGACAC |
| MCP-1 | TTAAAAACCTGGATCGGAACCAA | GCATTAGCTTCAGATTTACGGGT |
| TNF-a | CAGGCGGTGCCTATGTCTC | CGATCACCCCGAAGTTCAGTAG |
| Spp-1 | ATCTCACCATTCGGATGAGTCT | TGTAGGGACGATTGGAGTGAAA |
| ICAM-1 | GTGATGCTCAGGTATCCATCCA | CACAGTTCTCAAAGCACAGCG |

**Table 2**

F4/80 Staining Protocol for Macrophage Staining in ApoE Knockout Mouse Aorta

| primary Ab | Ab vendor | pretreatment | primary | staining system |
|---|---|---|---|---|
| rat anti – F 4/80 monoclonal | Biorad MCA497G Hercules, CA | proteinase K, rt, 3 min | 1:100 in NAD, 60 min | ProMark Rat on Mouse HRP Polymer:<br>15 min, probe<br>15 min, polymer<br>AEC, 5 min<br>CATHE hematoxylin 1:10, 1 min |